

Non-standard Higgs couplings in single Higgs boson production at the LHC and future linear collider

G. Akkaya Selçin^{1,2,*} and İ. Şahin^{1,†}

¹*Department of Physics, Faculty of Sciences,
Ankara University, 06100 Tandogan, Ankara, Turkey*

²*Department of Physics, Faculty of Arts and Sciences,
Bitlis Eren University, 13000 Bitlis, Turkey*

Abstract

We investigate the potential of single Higgs boson photoproduction at the LHC and at $e\gamma$ mode of future linear e^-e^+ collider to probe non-standard $HZ\gamma$ and $H\gamma\gamma$ couplings. We consider the semi-elastic production process $pp \rightarrow p\gamma p \rightarrow pHqX$ at the LHC where q represents the quarks and X represents the remnants of one of the initial protons. We also study the single Higgs production through $\gamma e \rightarrow He$ in the $e\gamma$ collision at the future linear collider. We perform a model-independent analysis and obtain the sensitivity bounds on the non-standard Higgs couplings for both colliders. We compare the capability of single Higgs photoproduction process at these two colliders to probe non-standard Higgs couplings.

*akkayag@ankara.edu.tr

†inancsahin@ankara.edu.tr

I. INTRODUCTION

The Higgs boson predicted by Standard Model (SM) of particle physics was discovered by ATLAS and CMS Collaborations at Large Hadron Collider (LHC) [1, 2]. After its discovery, intense experimental studies have been carried out to reveal its properties and couplings to other SM particles [3–5]. Precise determination of the Higgs couplings will either confirm the gauge structure of SM, or provide signal of new physics beyond SM. In this paper we investigate the non-standard couplings of the Higgs to gauge bosons Z and γ through semi-elastic production of the Higgs boson at the LHC and single production at $e\gamma$ mode of future linear e^-e^+ collider. These production processes are electroweak in nature and provide clean channels with respect to deep inelastic proton-proton collision at the LHC. Therefore, they can be used to perform precision measurements of the Higgs couplings.

Non-standard Higgs couplings to gauge bosons have been constrained through several Higgs decay processes at the LHC [3, 5–9]. There are also experimental constraints obtained from electroweak precision measurements at LEP and Tevatron [6–8, 10, 11]. One way to examine non-standard Higgs couplings is to employ the effective lagrangian method. In this method any contribution coming from new physics beyond SM is described by higher dimensional operators. These higher dimensional operators are added to the SM lagrangian and inversely proportional to some powers of Λ which is called the scale of new physics. In this paper we analyze non-standard $HZ\gamma$ and $H\gamma\gamma$ couplings in a model independent way by means of the effective lagrangian formalism of Refs.[6–8, 12–16]. There are five C and P even dimension-6 operators which modify the Higgs boson couplings to Z and γ bosons [6–8, 12–16]:

$$\begin{aligned}
\mathcal{O}_{WW} &= \Phi^\dagger \hat{W}_{\mu\nu} \hat{W}^{\mu\nu} \Phi \\
\mathcal{O}_{BB} &= \Phi^\dagger \hat{B}_{\mu\nu} \hat{B}^{\mu\nu} \Phi \\
\mathcal{O}_{BW} &= \Phi^\dagger \hat{B}_{\mu\nu} \hat{W}^{\mu\nu} \Phi \\
\mathcal{O}_W &= (D_\mu \Phi)^\dagger \hat{W}^{\mu\nu} (D_\nu \Phi) \\
\mathcal{O}_B &= (D_\mu \Phi)^\dagger \hat{B}^{\mu\nu} (D_\nu \Phi)
\end{aligned} \tag{1}$$

where Φ is the scalar doublet, D_μ is the covariant derivative, $\hat{W}_{\mu\nu} = i\frac{g}{2}(\vec{\sigma} \cdot \vec{W}_{\mu\nu})$ and $\hat{B}_{\mu\nu} = i\frac{g'}{2}B_{\mu\nu}$. Here g and g' are the $SU(2)_L$ and $U(1)_Y$ gauge couplings. The field strength tensors $W_{\mu\nu}^i$ and $B_{\mu\nu}$ belong to $SU(2)_L$ and $U(1)_Y$ gauge groups respectively. The SM lagrangian

is then modified by the following dimension-6 effective lagrangian:

$$\mathcal{L}_{eff} = \sum_n \frac{f_n}{\Lambda^2} \mathcal{O}_n \quad (2)$$

where f_n denote the non-standard couplings and Λ is the scale of new physics. After symmetry breaking, the effective lagrangian in Eq.(2) give rise to the following $HZ\gamma$ and $H\gamma\gamma$ interactions [6]:

$$\mathcal{L}_{eff} = g_{H\gamma\gamma} H A_{\mu\nu} A^{\mu\nu} + g_{HZ\gamma}^{(1)} A_{\mu\nu} Z^\mu \partial^\nu H + g_{HZ\gamma}^{(2)} H A_{\mu\nu} Z^{\mu\nu}. \quad (3)$$

where $V_{\mu\nu} = \partial_\mu V_\nu - \partial_\nu V_\mu$ with $V = A$ and Z field. The non-standard couplings $g_{H\gamma\gamma}$, $g_{HZ\gamma}^{(1)}$ and $g_{HZ\gamma}^{(2)}$ are related to the couplings f_n appearing in the effective lagrangian (2) before symmetry breaking as

$$g_{H\gamma\gamma} = - \left(\frac{gM_W}{\Lambda^2} \right) \frac{s^2(f_{BB} + f_{WW} - f_{BW})}{2} \quad (4)$$

$$g_{HZ\gamma}^{(1)} = \left(\frac{gM_W}{\Lambda^2} \right) \frac{s(f_W - f_B)}{2c} \quad (5)$$

$$g_{HZ\gamma}^{(2)} = \left(\frac{gM_W}{\Lambda^2} \right) \frac{s[2s^2 f_{BB} - 2c^2 f_{WW} + (c^2 - s^2) f_{BW}]}{2c} \quad (6)$$

where $s = \sin\theta_W$, $c = \cos\theta_W$, θ_W is the Weinberg angle and M_W is the mass of the W boson. In the calculations presented in this paper the energy scale of new physics is taken to be $\Lambda = 1\text{TeV}$. The effective operators in (1) contribute also HZZ and HWW couplings. Since the processes that we consider in this paper do not contain these couplings, we do not present the contributions coming from effective lagrangian (2) to HZZ and HWW . The effective operator \mathcal{O}_{BW} modifies also the $W^3 - B$ mixing. It is stringently restricted by the electroweak precision measurements [14, 15, 17]. Therefore, during the analysis we set $f_{BW} = 0$ and consider the contributions from four couplings f_{WW} , f_{BB} , f_W and f_B . For the purpose of simplicity, we will consider the following six different new physics scenarios:

$$\underline{\textit{Scenario I}} : f_B = f_W = 0, f_{BB} = f_{WW}$$

$$\underline{\textit{Scenario II}} : f_B = -f_W, f_{BB} = f_{WW} = 0$$

$$\underline{\textit{Scenario III}} : f_B = f_W = 0, f_{BB} = -f_{WW}$$

$$\underline{\textit{Scenario IV}} : f_B = f_W = 0, f_{WW} = \tan^2 \theta_W f_{BB}$$

$$\underline{\textit{Scenario V}} : f_W = f_{WW} = 0$$

$$\underline{\textit{Scenario VI}} : f_B = f_{BB} = 0$$

In scenarios I–IV we impose three constraints and therefore we have one free parameter. On the other hand, in scenarios V and VI two constraints are imposed and two parameters remain free. Here we should note the following important point: In this paper, we employ the set of bosonic operators in the Hagiwara-Ishihara-Szalapski-Zeppenfeld (HISZ) basis [15]. The operators \mathcal{O}_W and \mathcal{O}_B do not appear in the Warsaw basis [18]. They could be translated into other operators, including \mathcal{O}_{WW} , \mathcal{O}_{BW} , \mathcal{O}_{BB} and other dimension-6 operators. Therefore all five operators given in Eq.(1) are not independent. In scenarios I, III and IV we ignore the contributions from \mathcal{O}_W and \mathcal{O}_B operators which are absent in the Warsaw basis. In scenarios II, V and VI we consider the contributions from these operators. However, we consider at most two of the couplings as independent parameters. Therefore, our scenarios do not overwhelm the degrees of freedom in the effective lagrangian.

$HZ\gamma$ and $H\gamma\gamma$ interactions do not appear in the SM at the tree-level. However, they receive contributions at one-loop level. One-loop contributions to these interactions can be approximated to the following effective lagrangian [19, 20]:

$$\mathcal{L}_{eff} = g_{H\gamma\gamma}^{(SM)} H A_{\mu\nu} A^{\mu\nu} + g_{HZ\gamma}^{(SM)} H A_{\mu\nu} Z^{\mu\nu} \quad (7)$$

where, $g_{H\gamma\gamma}^{(SM)} = \frac{2\alpha}{9\pi\nu}$ and $g_{HZ\gamma}^{(SM)} = \frac{\alpha}{4\pi\nu\sin\theta_W}(5.508 - 0.004i)$. Here, α is the fine structure constant and ν is the electroweak vacuum expectation value.

The semi-elastic single Higgs boson production at the LHC has been studied in Refs.[21, 22]. However, in these studies only non-standard $HZ\gamma$ coupling has been taken into account. In our analysis of semi-elastic Higgs production we consider both non-standard $HZ\gamma$ and $H\gamma\gamma$ couplings. We do not assume that $HZ\gamma$ and $H\gamma\gamma$ couplings are independent from each other. We obtain bounds on f_n couplings of the operators (1) before symmetry breaking which contribute to both $HZ\gamma$ and $H\gamma\gamma$. The non-standard Higgs couplings to gauge bosons have also been investigated at future linear e^-e^+ collider and its $e\gamma$ and $\gamma\gamma$ modes [23–41]. The non-standard $HZ\gamma$ and $H\gamma\gamma$ interactions were investigated through single production process $\gamma e \rightarrow He$ in Refs.[24, 26]. In Ref.[26] the authors analyzed CP -odd interactions which are different from C and P even effective interactions that we consider. In Ref.[24] the authors considered a similar (but not equivalent) effective lagrangian for the non-standard Higgs interactions. The difference is that the effective interaction proportional to $g_{HZ\gamma}^{(1)}$ (see Eq. (3)) was omitted in Ref.[24]. Another difference between our work and that of [24] is that Ref.[24] was published long before the discovery of Higgs boson. Therefore,

the authors couldn't perform a detailed statistical analysis considering the exact value of the Higgs mass. In our analysis of single Higgs production $\gamma e \rightarrow He$, we perform a χ^2 test and estimate sensitivity of the linear collider based $e\gamma$ collider to non-standard Higgs couplings for various integrated luminosity values.

II. SINGLE HIGGS PRODUCTION THROUGH PHOTON-PROTON COLLISION AT THE LHC

The LHC is designed as a high-energy proton-proton collider and the majority of the studies at the LHC focused on deep inelastic scattering (DIS) processes where both of the colliding protons dissociate into partons. On the other hand, it was firstly shown experimentally at the Fermilab Tevatron that complementary to hadron-hadron collisions, hadron colliders can also be studied as a photon-photon and photon-hadron collider [42–44]. Recent experimental studies by CMS and ATLAS Collaborations have verified the existence of such photon-induced reactions at the LHC [45–49]. It was also shown that these photon-induced processes at the LHC have a significant potential to probe new physics beyond the SM [47–49]. The photon-photon collisions take place when both of the incoming protons emit quasireal photons. These emitted quasireal photons can interact mutually and the photon-photon collision occurs as a subprocess of the proton-proton collision. Similarly when one of the incoming proton emits a quasireal photon then a photon-proton collision can occur. These photon-proton collision processes are sometimes called semi-elastic processes due to their hybrid nature. Here, the essential point is the distinguishability of such photon-photon and photon-proton processes from those in which initial photons are described by propagators. According to equivalent photon approximation (EPA) [50–52], emitted photons have a very low virtuality and up to a high degree of approximation they are accepted to be real. Furthermore, since the virtuality of the quasireal photons is very low, photon emitting protons do not generally dissociate into partons but they remain intact [53, 54]. After elastic photon emission protons generally deviate slightly from the direction of beam pipe and escape from the central detectors without interacting. This causes a missing energy signature known as the forward large-rapidity gap, in the corresponding forward region of the central detector [53–55]. Moreover, the LHC is planned to be equipped with very forward detectors which can detect intact protons escaping from the central detectors [56–58]. The installa-

tion of very forward detectors should allow to separate more easily the photon-photon and photon-proton processes, where one or both of the incident protons remain intact [59–62]. The range of the forward detectors are characterized by the ξ parameter which represents the momentum fraction loss of the proton. If \vec{p} represents the initial proton's momentum and \vec{p}' represents forward proton's momentum after scattering then, ξ parameter is given by the formula $\xi \equiv (|\vec{p}| - |\vec{p}'|)/|\vec{p}|$. In this paper, we will consider a forward detector acceptance range of $0.015 < \xi < 0.15$ [56–58].

There is an increasing interest in probing new physics through photon-photon and photon-proton collision at the LHC. Phenomenological studies on this subject have been growing rapidly in recent years and cover a wide spectrum of new physics scenarios. It is impossible to cite all of the references here, but some representative ones might be Refs. [21, 22, 63–89]. The semi-elastic single Higgs boson production can be studied through the process $pp \rightarrow p\gamma p \rightarrow pHqX$ at the LHC. This process consists of the subprocesses $\gamma q \rightarrow Hq$ where q represents the quarks. We ignore the top quark distribution and consider 10 independent subprocess for $q = u, d, s, c, b, \bar{u}, \bar{d}, \bar{s}, \bar{c}, \bar{b}$. In the presence of non-standard $HZ\gamma$ and $H\gamma\gamma$ interactions the subprocess $\gamma q \rightarrow Hq$ is described by the Feynman diagrams given in Fig.1. The semi-elastic process $pp \rightarrow p\gamma p \rightarrow pHqX$ consists of two different types of proton scattering; elastic photon emission takes place from one of the initial protons, whereas other initial proton interact strongly with the emitted photon and undergoes an inelastic scattering (Fig.2). Therefore, the cross section for the semi-elastic process $pp \rightarrow p\gamma p \rightarrow pHqX$ is obtained by integrating the cross sections for the subprocesses over the photon and quark distributions:

$$\sigma(pp \rightarrow p\gamma p \rightarrow pHqX) = \sum_q \int_{x_{1min}}^{x_{1max}} dx_1 \int_0^1 dx_2 \left(\frac{dN_\gamma}{dx_1} \right) \left(\frac{dN_q}{dx_2} \right) \hat{\sigma}_{\gamma q \rightarrow Hq}(\hat{s}). \quad (8)$$

Here, $\frac{dN_\gamma}{dx_1}$ and $\frac{dN_q}{dx_2}$ are the equivalent photon and quark distribution functions, respectively. The quark distribution functions can be evaluated numerically by using the code MSTW2008 [90]. In Eq.(8) the integral variable x_1 is the energy fraction that represents the ratio between the emitted equivalent photon and initial proton energy. The other variable x_2 represents the momentum fraction of the proton's momentum carried by the quark. The equivalent photon distribution $\frac{dN_\gamma}{dx_1}$ is given by an analytical expression. We do not give its explicit form. Its explicit form can be found in the literature (for example see [50] or [66]). At the LHC energies where the energy of the incoming proton is much greater than its mass ($E \gg m_p$),

the ξ parameter is approximated as $\xi \approx \frac{E-E'}{E} = \frac{E_\gamma}{E} = x_1$. Here, E and E' are the energy of the initial and final (scattered) proton and E_γ is the energy of the equivalent photon. Therefore, the upper and lower limits of the dx_1 integration are determined by the limits of the forward detector acceptance and we take $x_{1min} = \xi_{min} = 0.015$, $x_{1max} = \xi_{max} = 0.15$.

In Figs.3-6, we plot the total cross section of the process $pp \rightarrow p\gamma p \rightarrow pHqX$ as a function of non-standard Higgs couplings for scenarios I-IV. In addition to new physics contributions we have also considered the effective lagrangian (7) that contains SM one-loop contributions. For a concrete result we have obtained 95% confidence level (C.L.) bounds on non-standard couplings using the simple χ^2 criterion. The χ^2 function is given by

$$\chi^2 = \left(\frac{N_{NS} - N_{SM}}{N_{SM} \delta} \right)^2 \quad (9)$$

where, N_{NS} is the number of events containing both new physics and SM contributions, N_{SM} is the number of events expected in the SM and $\delta = \frac{1}{\sqrt{N_{SM}}}$ is the statistical error. The number of events has been calculated considering the $H \rightarrow b\bar{b}$ decay of the Higgs boson as the signal. Hence, we assume that $N_{NS(SM)} = E \times S \times L_{int} \times \sigma_{NS(SM)} \times BR$ where, E is the b-tagging efficiency, S is the survival probability factor, L_{int} is the integrated luminosity and BR is the branching ratio for $H \rightarrow b\bar{b}$. σ_{SM} represents the SM cross section and σ_{NS} represents the cross section containing both new physics and SM contributions. We have taken into account a b-tagging efficiency of $E = 0.6$, survival probability factor of $S = 0.7$ and branching ratio of $BR = 0.6$. The survival probability factor of 0.7 was proposed for the single W boson photoproduction [91, 92]. We assume that same survival probability factor is valid for our process. Although the b-tagging efficiency is not constant but depends on many different parameters such as the jet transverse momentum, the algorithm used in the detector, etc. we assume a constant b-tagging efficiency of 0.6. According to experimental works a constant average value of 0.6 for b-tagging efficiency is reasonable [93]. We have also placed a pseudorapidity cut of $|\eta| < 2.5$ for final state particles. There are background processes which contribute to the same final state. The background processes consist of the SM subprocesses that contribute to $pp \rightarrow p\gamma p \rightarrow pb\bar{b}qX$. There are totally 18 background subprocess of the type $\gamma q \rightarrow k, b, \bar{b}$ where, $q = u, d, s, c, b, \bar{u}, \bar{d}, \bar{s}, \bar{c}, \bar{b}$ and $k = u, d, s, c, b, t, \bar{u}, \bar{d}, \bar{s}, \bar{c}, \bar{b}, \bar{t}$ quarks. The background contributions have been calculated by using CalcHEP 3.6.20 [94]. The determination of an on-shell Higgs boson with mass approximately 125 GeV requires an invariant mass measurement of the final-state $b\bar{b}$ pairs. If we impose a cut and demand

that the invariant mass of the $b\bar{b}$ pairs is in the interval $120 \text{ GeV} < M_{b\bar{b}} < 130 \text{ GeV}$ then the background cross section is reduced considerably and gives $\sigma_{\text{background}} = 0.05 \text{ pb}$. Since the background contribution cannot be discerned from Higgs production cross section, during statistical analysis we add the background contribution to the SM cross section and assume that $\sigma_{NS(SM)} = \sigma(pp \rightarrow p\gamma p \rightarrow pHqX)_{NS(SM)} + \frac{1}{BR} \times \sigma_{\text{background}}$. Here, the factor $\frac{1}{BR}$ is used to cancel out the branching ratio in $N_{NS(SM)}$.

In Table I we present 95% C.L. bounds on non-standard f_{ww}, f_w and f_{bb} couplings for scenarios I-IV. The bounds are obtained via one-parameter χ^2 analysis and we consider the integrated luminosity values of $L_{int} = 10, 30, 50, 100, 200 \text{ fb}^{-1}$. For scenarios V and VI we have two free coupling parameters and therefore the bounds are obtained using two-parameter χ^2 analysis. In Fig.7 and Fig.8, we plot 95% C.L. bounds on two dimensional parameter spaces $f_B - f_{BB}$ and $f_W - f_{WW}$ for scenarios V and VI respectively.

The CMS collaboration at the LHC has determined direct experimental bounds on non-standard Higgs-gauge boson couplings by studying Higgs boson decay to ZZ , $Z\gamma$, $\gamma\gamma$ and WW [5]. The following 95% C.L. bounds have been given on the ratio of $HZ\gamma$ and $H\gamma\gamma$ couplings to HZZ : $-0.046 < \frac{a_2^{Z\gamma}}{a_1} < 0.044$ and $-0.011 < \frac{a_2^{\gamma\gamma}}{a_1} < 0.054$ [5]. Here, a couplings are defined by $a_1 = 2g_{HZZ}/m_Z^2$, $a_2^{Z\gamma} = g_{HZ\gamma}^{(2)}$ and $a_2^{\gamma\gamma} = 2g_{H\gamma\gamma}$, where $g_{H\gamma\gamma}$ and $g_{HZ\gamma}^{(2)}$ are the couplings in the effective lagrangian in Eq.(3) and g_{HZZ} is the coupling of the Higgs to two Z boson, i.e., $g_{HZZ}H Z^\mu Z_\mu$. If we assume that g_{HZZ} coupling is equal to its SM value ($g_{HZZ} = m_Z^2/\nu$; $\nu = 246 \text{ GeV}$) then we can extract the experimental bounds on the couplings $g_{HZ\gamma}^{(2)}$ and $g_{H\gamma\gamma}$. The scenario III and scenario IV isolate the couplings $g_{HZ\gamma}^{(2)}$ and $g_{H\gamma\gamma}$ respectively. Therefore, these scenarios give us the opportunity to compare our bounds with the experimental bounds of Ref.[5]. In scenario III, the experimental bound on $\frac{a_2^{Z\gamma}}{a_1}$ can be converted to the bounds on f couplings as $-13 < f_{BB} < 12.6$ and $-12.6 < f_{WW} < 13$. Similarly, in scenario IV the experimental bound on $\frac{a_2^{\gamma\gamma}}{a_1}$ can be converted as $-5.67 < f_{BB} < 27.83$ and $-1.7 < f_{WW} < 8.35$. When we compare these bounds with the corresponding bounds given in Table I, we see that our bounds for the integrated luminosity of 200 fb^{-1} are approximately a factor of 3 better than the experimental bounds in the case of scenario III and approximately a factor of 2.5 better in the case of scenario IV.

III. SINGLE HIGGS PRODUCTION THROUGH PHOTON-ELECTRON COLLISION AT THE FUTURE LINEAR COLLIDER

The non-standard $H\gamma\gamma$ and $HZ\gamma$ couplings can be investigated with a high precision at future linear e^-e^+ collider and its $e\gamma$ and $\gamma\gamma$ modes. We consider the single Higgs production in the $e\gamma$ collision via the subprocess $\gamma e \rightarrow He$. The tree-level Feynman diagrams for $\gamma e \rightarrow He$ is very similar to that of Fig.1, but we should replace quarks with electrons (or positrons), $q \rightarrow e$. The initial photon beam can be obtained through equivalent photon emission from incoming electron or positron beam, similar to equivalent photon emission from protons at the LHC. However in the case of future linear collider, we have a more appealing option. A real photon beam can be obtained through Compton backscattering of laser light off the linear electron beam. Contrary to EPA, Compton backscattering provides an increasing photon spectrum as a function of the energy fraction $y = E_\gamma/E_e$, where E_γ and E_e represent the energy of the backscattered photon and initial electron beam, respectively [95, 96]. The backscattered photon spectrum is given by [95, 96]

$$f_{\gamma/e}(y) = \frac{1}{g(\zeta)} \left[1 - y + \frac{1}{1-y} - \frac{4y}{\zeta(1-y)} + \frac{4y^2}{\zeta^2(1-y)^2} \right] \quad (10)$$

where,

$$g(\zeta) = \left(1 - \frac{4}{\zeta} - \frac{8}{\zeta^2} \right) \ln(\zeta + 1) + \frac{1}{2} + \frac{8}{\zeta} - \frac{1}{2(\zeta + 1)^2}. \quad (11)$$

Here, $\zeta = 4E_e E_0/M_e^2$ and E_0 is the energy of initial laser photon before Compton backscattering. The ζ parameter can be taken to be $\zeta = 4.8$ in which case the backscattered photon energy is maximized without spoiling the luminosity. Then, the upper limit of the energy fraction becomes $y_{max} = 0.83$. The process $\gamma e \rightarrow He$ takes part as a subprocess in the main e^-e^+ collision. Therefore, the total cross section observed in the e^-e^+ collision can be obtained by integrating the cross section for $\gamma e \rightarrow He$ over the backscattered photon spectrum:

$$\sigma_{e^-e^+} = \int_{y_{min}}^{0.83} f_{\gamma/e}(y) \sigma_{\gamma e \rightarrow He} dy \quad (12)$$

where, $y_{min} = \frac{m_H^2}{s}$ and s is the Mandelstam parameter of the e^-e^+ collision. The behavior of the total cross section as a function of non-standard Higgs couplings is shown in Figs.9-12 for scenarios I-IV. In these figures, the center of mass energy of the main e^-e^+ collider is taken

to be $\sqrt{s} = 0.5$ TeV. Since the mass of the electron is very tiny the tree-level SM contribution to the process $\gamma e \rightarrow He$ can be safely neglected. Therefore the SM contributions to $\gamma e \rightarrow He$ are coming from the loop-level. We consider SM one-loop contributions described by the effective lagrangian (7).

Using the simple χ^2 criterion we estimate sensitivity of the linear collider-based $e\gamma$ collider to non-standard Higgs couplings for the integrated luminosity values of $L_{int} = 10, 30, 50, 100, 200 \text{ fb}^{-1}$ and $\sqrt{s} = 0.5$ TeV. We consider $H \rightarrow b\bar{b}$ decay channel of the Higgs boson and assume that $b\bar{b}$ final state with invariant mass in the interval $120 \text{ GeV} < M_{b\bar{b}} < 130 \text{ GeV}$ is identified as the signal. In the χ^2 function the number of events is given by $N_{NS(SM)} = E \times L_{int} \times \sigma_{NS(SM)} \times BR$. We take into account a b-tagging efficiency of $E = 0.6$ and branching ratio of $BR = 0.6$. We assume that the central detectors have a pseudorapidity coverage of $|\eta| < 2.5$. Therefore, we place a cut of $|\eta| < 2.5$ for all final state particles. The potential background process is $\gamma e \rightarrow b\bar{b}e$. It is described by 8 tree-level Feynman diagrams and gives a total cross section of $\sigma_{\text{background}} = 4.1 \times 10^{-3} \text{ pb}$ after imposing the cuts $120 \text{ GeV} < M_{b\bar{b}} < 130 \text{ GeV}$ and $|\eta| < 2.5$. Similar to the statistical analysis performed in the previous section, we assume that the background contribution cannot be discerned from Higgs production. Therefore, during statistical analysis we add the background contribution to the SM cross section and assume that $\sigma_{NS(SM)} = (\sigma_{e-e+})_{NS(SM)} + \frac{1}{BR} \times \sigma_{\text{background}}$ where $(\sigma_{e-e+})_{NS(SM)}$ is the integrated cross section defined in (12). The subscript NS represents the cross section containing both new physics and SM contributions and subscript SM represents the SM cross section alone. The 95% C.L. bounds on non-standard f_{ww}, f_w and f_{bb} couplings are given in Table II for scenarios I-IV. We observe from Tables I and II that the bounds of Table II are more restrictive with respect to the corresponding bounds of Table I. The average improvement factors are approximately 6 for scenario I, 3 for scenarios II and III and 8.5 for scenario IV. For scenarios V and VI the bounds are obtained in the two-dimensional parameter spaces $f_B - f_{BB}$ and $f_W - f_{WW}$. The 95% C.L. restricted regions in these parameter spaces are given in Fig.13 and Fig.14. When we compare the bounds of Figs.13 and 14 with the similar LHC bounds given in Figs.7 and 8, we see that the bounds of the linear collider are approximately a factor of 5 better than the corresponding bounds of the LHC.

We can also compare the bounds of future linear collider with the current experimental bounds. The CMS bounds on f_{BB} and f_{WW} couplings have been given in the last paragraph

of the previous section. When we compare these experimental bounds with the corresponding bounds given in Table II, we see that our bounds for the integrated luminosity of 200 fb^{-1} are approximately a factor of 8 better than the experimental bounds in the case of scenario III and approximately a factor of 20 better in the case of scenario IV.

IV. CONCLUSIONS

One of the prominent motivations of the future e^-e^+ collider is that it provides clean experimental environment which allows to make high precision measurements [97, 98]. In deep inelastic hadron-hadron collisions, initial hadron beams dissociate into partons and create myriad of jets which cause uncertainties and make it difficult to discern the signals that we want to observe. Moreover, in hadron colliders there are systematic uncertainties arising from the proton structure functions, from unknown higherorder perturbative QCD corrections, and from nonperturbative QCD effects [98]. Lepton colliders do not suffer from these kind of uncertainties, and the level of precision is expected to be enhanced considerably compared to hadron colliders. On the other hand, ultraperipheral collisions in a hadron collider provides a unique opportunity to search for the physics beyond the SM in a rather clean environment with respect to deep inelastic hadron-hadron collisions. Exclusive and semielastic processes are examples of the reactions in an ultraperipheral collision. In semi-elastic Higgs production $pp \rightarrow p\gamma p \rightarrow pHqX$ only one of the incoming proton dissociates into partons but the other proton remains intact. The absence of the remnants of one of the proton beam, allows to discern the signal more easily. Furthermore, tagging the intact scattered protons in the forward detectors allows us to reconstruct quasireal photons' momenta. The knowledge obtained in this way is very useful in reconstructing the kinematics of the reaction. The semi-elastic Higgs production is electroweak in nature and free from backgrounds containing strong interaction. Due to above reasons, the uncertainties associated with the Higgs detection for $pp \rightarrow p\gamma p \rightarrow pHqX$ are expected to be reduced considerably compared to deep inelastic processes at the LHC. Therefore, the comparison of the results obtained in semi-elastic production at the LHC and future e^-e^+ collider is important and contributes to the physics program of the future e^-e^+ collider.

In the paper, we consider similar subprocesses $\gamma q \rightarrow Hq$ and $\gamma e \rightarrow He$ at the LHC and at future e^-e^+ collider. We investigate the potential of these two colliders to probe

non-standard Higgs couplings. We show that $e\gamma$ mode of the linear collider with center of mass energy of $\sqrt{s} = 0.5$ TeV probes the non-standard $HZ\gamma$ and $H\gamma\gamma$ couplings with better sensitivity than the γ -proton collision at the LHC. The improvement factor depends on the coupling and the luminosity, but roughly the bounds are improved by a factor of 5.

-
- [1] G. Aad *et al.* [ATLAS Collaboration], Phys. Lett. B **716**, 1 (2012) [arXiv:1207.7214 [hep-ex]].
 - [2] S. Chatrchyan *et al.* [CMS Collaboration], Phys. Lett. B **716**, 30 (2012) [arXiv:1207.7235 [hep-ex]].
 - [3] G. Aad *et al.* [ATLAS Collaboration], Phys. Lett. B **726** (2013) 88 Erratum: [Phys. Lett. B **734** (2014) 406] [arXiv:1307.1427 [hep-ex]].
 - [4] S. Chatrchyan *et al.* [CMS Collaboration], Phys. Rev. Lett. **110**, no. 8, 081803 (2013) [arXiv:1212.6639 [hep-ex]].
 - [5] V. Khachatryan *et al.* [CMS Collaboration], Phys. Rev. D **92**, 012004 (2015) [arXiv:1411.3441 [hep-ex]].
 - [6] T. Corbett, O. J. P. Eboli, J. Gonzalez-Fraile and M. C. Gonzalez-Garcia, Phys. Rev. D **86**, 075013 (2012) [arXiv:1207.1344 [hep-ph]].
 - [7] T. Corbett, O. J. P. Eboli, J. Gonzalez-Fraile and M. C. Gonzalez-Garcia, Phys. Rev. D **87**, 015022 (2013) [arXiv:1211.4580 [hep-ph]].
 - [8] E. Masso and V. Sanz, Phys. Rev. D **87**, 033001 (2013) [arXiv:1211.1320 [hep-ph]].
 - [9] S. Banerjee, S. Mukhopadhyay and B. Mukhopadhyaya, Phys. Rev. D **89**, 053010 (2014) [arXiv:1308.4860 [hep-ph]].
 - [10] A. Gutierrez-Rodriguez, J. Montano and M. A. Perez, J. Phys. G **38**, 095003 (2011) [arXiv:1009.4354 [hep-ph]].
 - [11] [The TEVNPH Working Group for the CDF and D0 Collaborations], arXiv:1207.0449 [hep-ex].
 - [12] W. Buchmuller and D. Wyler, Nucl. Phys. B **268**, 621 (1986).
 - [13] C. N. Leung, S. T. Love and S. Rao, Z. Phys. C **31**, 433 (1986).
 - [14] A. De Rujula, M. B. Gavela, P. Hernandez and E. Masso, Nucl. Phys. B **384**, 3 (1992).
 - [15] K. Hagiwara, S. Ishihara, R. Szalapski and D. Zeppenfeld, Phys. Rev. D **48**, 2182 (1993).
 - [16] M. C. Gonzalez-Garcia, Int. J. Mod. Phys. A **14**, 3121 (1999) [hep-ph/9902321].
 - [17] S. Alam, S. Dawson and R. Szalapski, Phys. Rev. D **57**, 1577 (1998) [hep-ph/9706542].

- [18] B. Grzadkowski, M. Iskrzynski, M. Misiak and J. Rosiek, JHEP **1010**, 085 (2010) [arXiv:1008.4884 [hep-ph]].
- [19] J. F. Donoghue, E. Golowich and B. R. Holstein, “Dynamics of the Standard Model,” Cambridge University Press, United Kingdom (2014).
- [20] M. Farina, Y. Grossman and D. J. Robinson, Phys. Rev. D **92**, 073007 (2015) [arXiv:1503.06470 [hep-ph]].
- [21] A. Senol, A. T. Tasci, I. T. Cakir and O. Cakir, Mod. Phys. Lett. A **29**, no. 36, 1450186 (2014) [arXiv:1405.6050 [hep-ph]].
- [22] S. Taheri Monfared, S. Fayazbakhsh and M. Mohammadi Najafabadi, Phys. Lett. B **762**, 301 (2016) [arXiv:1610.02883 [hep-ph]].
- [23] M. C. Gonzalez-Garcia, S. M. Lietti and S. F. Novaes, Phys. Rev. D **59**, 075008 (1999) [hep-ph/9811373].
- [24] A. T. Banin, I. F. Ginzburg and I. P. Ivanov, Phys. Rev. D **59**, 115001 (1999) [hep-ph/9806515].
- [25] K. Hagiwara, S. Ishihara, J. Kamoshita and B. A. Kniehl, Eur. Phys. J. C **14**, 457 (2000) [hep-ph/0002043].
- [26] I. F. Ginzburg and I. P. Ivanov, Eur. Phys. J. C **22**, 411 (2001) [hep-ph/0004069].
- [27] T. Han and J. Jiang, Phys. Rev. D **63**, 096007 (2001) [hep-ph/0011271].
- [28] V. Barger, T. Han, P. Langacker, B. McElrath and P. Zerwas, Phys. Rev. D **67**, 115001 (2003) [hep-ph/0301097].
- [29] T. Han, Y. P. Kuang and B. Zhang, Phys. Rev. D **73**, 055010 (2006) [hep-ph/0512193].
- [30] S. S. Biswal, R. M. Godbole, R. K. Singh and D. Choudhury, Phys. Rev. D **73**, 035001 (2006) Erratum: [Phys. Rev. D **74**, 039904 (2006)] [hep-ph/0509070].
- [31] D. Choudhury and Mamta, Phys. Rev. D **74**, 115019 (2006) [hep-ph/0608293].
- [32] İ. Şahin, Phys. Rev. D **77**, 115010 (2008) [arXiv:0802.0293 [hep-ph]].
- [33] S. Dutta, K. Hagiwara and Y. Matsumoto, Phys. Rev. D **78**, 115016 (2008) [arXiv:0808.0477 [hep-ph]].
- [34] B. Şahin, J. Phys. G **36**, 025012 (2009) [arXiv:0808.0842 [hep-ph]].
- [35] S. S. Biswal, D. Choudhury, R. M. Godbole and Mamta, Phys. Rev. D **79**, 035012 (2009) [arXiv:0809.0202 [hep-ph]].
- [36] S. S. Biswal and R. M. Godbole, Phys. Lett. B **680**, 81 (2009) [arXiv:0906.5471 [hep-ph]].

- [37] M. Beneke, D. Boito and Y. M. Wang, JHEP **1411**, 028 (2014) [arXiv:1406.1361 [hep-ph]].
- [38] Q. H. Cao, H. R. Wang and Y. Zhang, Chin. Phys. C **39**, no. 11, 113102 (2015) [arXiv:1505.00654 [hep-ph]].
- [39] S. Kumar, P. Poulose and S. Sahoo, Phys. Rev. D **91**, no. 7, 073016 (2015) [arXiv:1501.03283 [hep-ph]].
- [40] S. F. Ge, H. J. He and R. Q. Xiao, JHEP **1610**, 007 (2016) [arXiv:1603.03385 [hep-ph]].
- [41] S. Alam, S. Bebera, S. Kumar and S. Sahoo, arXiv:1701.08250 [hep-ph].
- [42] A. Abulencia *et al.* (CDF Collaboration), Phys. Rev. Lett. **98**, 112001 (2007); arXiv:hep-ex/0611040.
- [43] T. Aaltonen *et al.* (CDF Collaboration), Phys. Rev. Lett. **102**, 222002 (2009); arXiv:0902.2816 [hep-ex].
- [44] T. Aaltonen *et al.* (CDF Collaboration), Phys. Rev. Lett. **102**, 242001 (2009); arXiv:0902.1271 [hep-ex].
- [45] S. Chatrchyan *et al.* (CMS Collaboration), JHEP **1201**, 052 (2012) [arXiv:1111.5536 [hep-ex]].
- [46] S. Chatrchyan *et al.* (CMS Collaboration), JHEP **1211**, 080 (2012) [arXiv:1209.1666 [hep-ex]].
- [47] S. Chatrchyan *et al.* (CMS Collaboration), JHEP **1307**, 116 (2013) [arXiv:1305.5596 [hep-ex]].
- [48] V. Khachatryan *et al.* [CMS Collaboration], JHEP **1608**, 119 (2016) [arXiv:1604.04464 [hep-ex]].
- [49] M. Aaboud *et al.* [ATLAS Collaboration], Phys. Rev. D **94**, no. 3, 032011 (2016) [arXiv:1607.03745 [hep-ex]].
- [50] V. M. Budnev, I. F. Ginzburg, G. V. Meledin and V. G. Serbo, Phys. Rep. **15**, 181 (1975).
- [51] G. Baur *et al.*, Phys. Rep. **364**, 359 (2002).
- [52] K. Piotrkowski, Phys. Rev. D **63**, 071502 (2001) [hep-ex/0009065].
- [53] X. Rouby, Ph.D. thesis, Universite Catholique de Louvain [CERN-THESIS-2009-216 and CMS-TS-2009-004]
- [54] N. Schul, Ph.D. thesis, Universite Catholique de Louvain [CERN-THESIS-2011-271 and CMS-TS-2011-030].
- [55] M. Albrow *et al.* (CMS Collaboration), JINST **4**, P10001 (2009) [arXiv:0811.0120 [hep-ex]].
- [56] ATLAS Collaboration, CERN-LHCC-2011-012.
- [57] CMS and TOTEM collaboration, CERN-LHCC-2014-021.
- [58] M. Tasevsky [ATLAS Collaboration], AIP Conf. Proc. **1654**, 090001 (2015).

- [59] M. G. Albrow *et al.* (FP420 R and D Collaboration), JINST **4**, T10001 (2009) [arXiv:0806.0302 [hep-ex]].
- [60] M. Tasevsky, Nucl. Phys. Proc. Suppl. **179-180**, 187 (2008).
- [61] M. G. Albrow, T. D. Coughlin and J. R. Forshaw, Prog. Part. Nucl. Phys. **65**, 149 (2010) [arXiv:1006.1289 [hep-ph]].
- [62] M. Tasevsky, Int. J. Mod. Phys. A **29**, 1446012 (2014) [arXiv:1407.8332 [hep-ph]].
- [63] I. F. Ginzburg and A. Schiller, Phys. Rev. D **60**, 075016 (1999) [hep-ph/9903314].
- [64] V.A. Khoze, A.D. Martin and M.G. Ryskin, Eur. Phys. J. C **23**, 311 (2002); arXiv:hep-ph/0111078.
- [65] N. Schul and K. Piotrkowski, Nucl. Phys. B, Proc. Suppl., **179**, 289 (2008); arXiv:0806.1097 [hep-ph].
- [66] O. Kepka and C. Royon, Phys. Rev. D **78**, 073005 (2008); arXiv:0808.0322 [hep-ph].
- [67] İ. Şahin and S. C. İnan, JHEP **09**, 069 (2009); arXiv:0907.3290 [hep-ph].
- [68] T. Dougall and S. D. Wick, Eur. Phys. J. A **39**, 213 (2009) [arXiv:0706.1042 [hep-ph]].
- [69] M. Chaichian, P. Hoyer, K. Huitu, V. A. Khoze and A. D. Pilkington, JHEP **0905**, 011 (2009) [arXiv:0901.3746 [hep-ph]].
- [70] E. Chapon, C. Royon and O. Kepka, Phys. Rev. D **81**, 074003 (2010); arXiv:0912.5161 [hep-ph].
- [71] K. Piotrkowski and N. Schul, AIP Conf. Proc. **1200**, 434 (2010) [arXiv:0910.0202 [hep-ph]].
- [72] S. C. İnan, Phys. Rev. D **81**, 115002 (2010); arXiv:1005.3432 [hep-ph].
- [73] S. Atağ and A. A. Billur, JHEP **11**, 060 (2010); arXiv:1005.2841 [hep-ph].
- [74] V. P. Goncalves and W. K. Sauter, Phys. Rev. D **82**, 056009 (2010) [arXiv:1007.5487 [hep-ph]].
- [75] S. C. İnan and A. A. Billur, Phys. Rev. D **84**, 095002 (2011).
- [76] İ. Şahin, and A. A. Billur, Phys. Rev. D **83**, 035011 (2011); arXiv:1101.4998 [hep-ph].
- [77] İ. Şahin, and M. Koksalsal, JHEP **03**, 100 (2011); arXiv:1010.3434 [hep-ph].
- [78] R. S. Gupta, Phys. Rev. D **85**, 014006 (2012) [arXiv:1111.3354 [hep-ph]].
- [79] L. N. Epele, H. Fanchiotti, C. A. G. Canal, V. A. Mitsou and V. Vento, Eur. Phys. J. Plus **127**, 60 (2012) [arXiv:1205.6120 [hep-ph]].
- [80] B. Şahin and A. A. Billur, Phys. Rev. D **86**, 074026 (2012) [arXiv:1210.3235 [hep-ph]].
- [81] İ. Şahin *et al.*, Phys. Rev. D **88**, 095016 (2013) [arXiv:1304.5737 [hep-ph]].
- [82] M. Koksalsal and S. C. İnan, Adv. High Energy Phys. **2014**, 935840, (2014) [arXiv:1305.7096

- [hep-ph]].
- [83] H. Sun and C. X. Yue, Eur. Phys. J. C **74**, 2823 (2014) [arXiv:1401.0250 [hep-ph]].
 - [84] H. Sun, Eur. Phys. J. C **74**, 2977 (2014) [arXiv:1406.3897 [hep-ph]].
 - [85] S. Fichet, G. von Gersdorff, O. Kepka, B. Lenzi, C. Royon and M. Saimpert, Phys. Rev. D **89**, 114004 (2014) [arXiv:1312.5153 [hep-ph]].
 - [86] S. Fichet and G. von Gersdorff, JHEP **1403**, 102 (2014) [arXiv:1311.6815 [hep-ph]].
 - [87] A. Senol and M. Koksul, Phys. Lett. B **742**, 143 (2015) [arXiv:1410.3648 [hep-ph]].
 - [88] S. Fichet, G. von Gersdorff, B. Lenzi, C. Royon and M. Saimpert, JHEP **1502**, 165 (2015) [arXiv:1411.6629 [hep-ph]].
 - [89] S. Fichet, G. von Gersdorff and C. Royon, Phys. Rev. Lett. **116**, no. 23, 231801 (2016) [arXiv:1601.01712 [hep-ph]].
 - [90] A. D. Martin, W. J. Stirling, R. S. Thorne and G. Watt, Eur. Phys. J. C **63**, 189 (2009) [arXiv:0901.0002 [hep-ph]].
 - [91] J. de Favereau de Jeneret, V. Lemaitre, Y. Liu, S. Ovin, T. Pierzchala, K. Piotrkowski, X. Rouby, N. Schul and M. Vander Donckt, arXiv:0908.2020 [hep-ph].
 - [92] V. A. Khoze, A. D. Martin and M. G. Ryskin, Eur. Phys. J. C **24**, 459 (2002) [hep-ph/0201301].
 - [93] G. Aad *et al.* [ATLAS Collaboration], JINST **11**, no. 04, P04008 (2016) [arXiv:1512.01094 [hep-ex]].
 - [94] A. Belyaev, N. D. Christensen and A. Pukhov, Comput. Phys. Commun. **184**, 1729 (2013) [arXiv:1207.6082 [hep-ph]].
 - [95] I.F. Ginzburg *et al.*, Nucl. Instrum. Methods **205**, 47 (1983).
 - [96] I.F. Ginzburg *et al.*, Nucl. Instrum. Methods **219**, 5 (1984).
 - [97] T. Behnke *et al.*, “The International Linear Collider Technical Design Report - Volume 1: Executive Summary,” arXiv:1306.6327 [physics.acc-ph].
 - [98] H. Baer *et al.*, “The International Linear Collider Technical Design Report - Volume 2: Physics,” arXiv:1306.6352 [hep-ph].

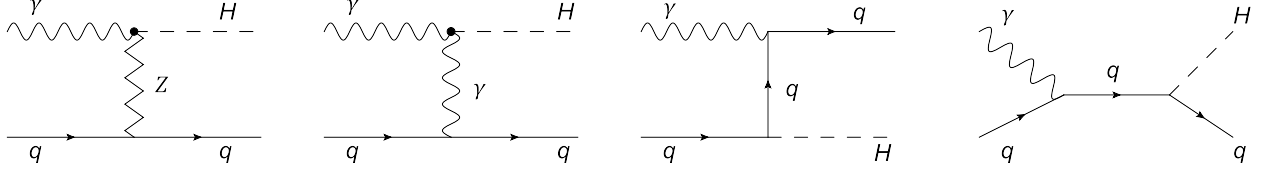


FIG. 1: Tree-level Feynman diagrams for the subprocess $\gamma q \rightarrow Hq$

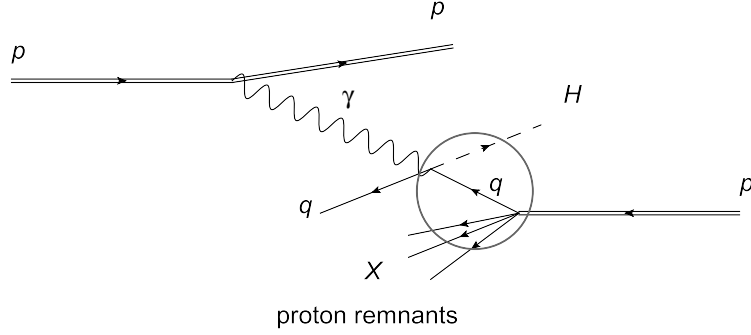


FIG. 2: The illustration of the process $pp \rightarrow p\gamma p \rightarrow pHqX$.

TABLE I: 95% C.L. bounds on f_{ww}, f_w and f_{bb} for various integrated LHC luminosities and scenarios. Bounds are given in units of TeV^{-2} . The center of mass energy of the proton-proton system is taken to be $\sqrt{s} = 14\text{TeV}$.

Luminosity	(Scenario-I) f_{ww}	(Scenario-II) f_w	(Scenario-III) f_{bb}	(Scenario-IV) f_{bb}
$10fb^{-1}$	(-6.3,7.9)	(-19.8,15.4)	(-9.9,7.7)	(-13.2,15.6)
$30fb^{-1}$	(-4.6,6.2)	(-15.6,11.3)	(-7.8,5.6)	(-9.8,12.2)
$50fb^{-1}$	(-3.9,5.6)	(-14.1,9.7)	(-7.0,4.9)	(-8.5,10.8)
$100fb^{-1}$	(-3.2,4.8)	(-12.2,7.9)	(-6.1,3.9)	(-7.0,9.3)
$200fb^{-1}$	(-2.6,4.2)	(-10.7,6.4)	(-5.3,3.2)	(-5.7,8.1)

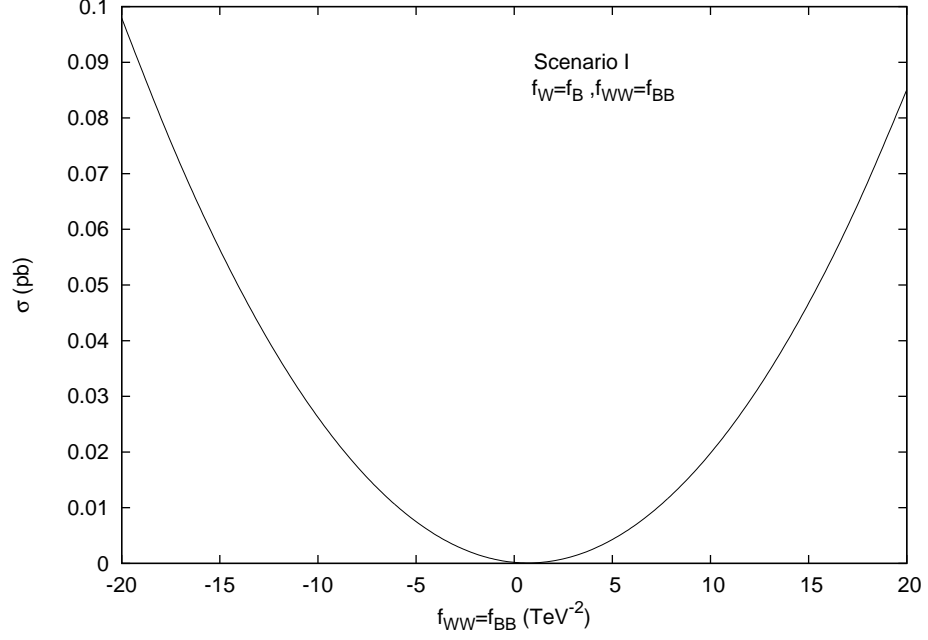


FIG. 3: The total cross section of the process $pp \rightarrow p\gamma p \rightarrow pHqX$ as a function of non-standard Higgs coupling for scenario I. The center of mass energy of the proton-proton system is taken to be $\sqrt{s} = 14\text{TeV}$.

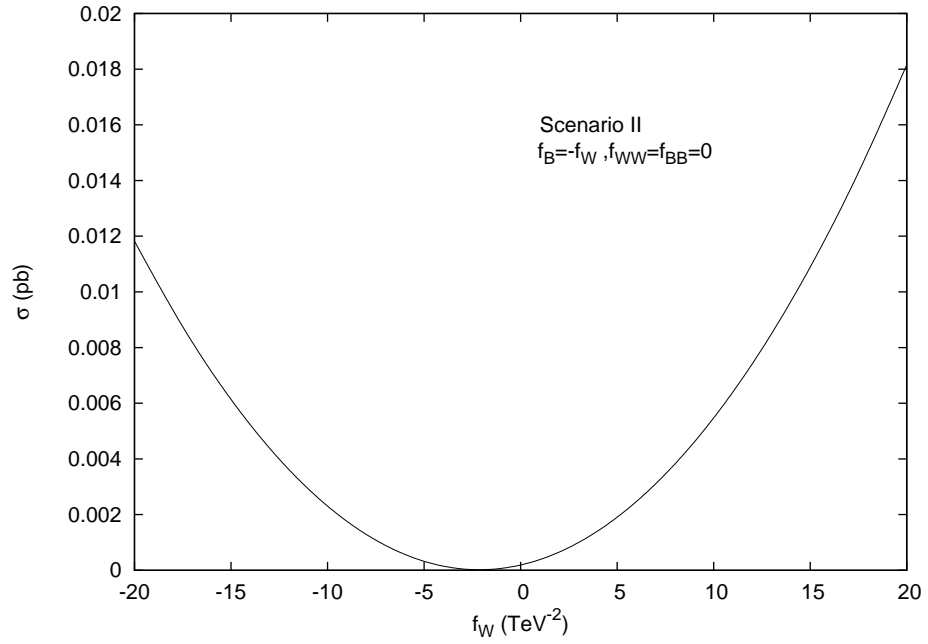


FIG. 4: The same as Fig.3 but for scenario II.

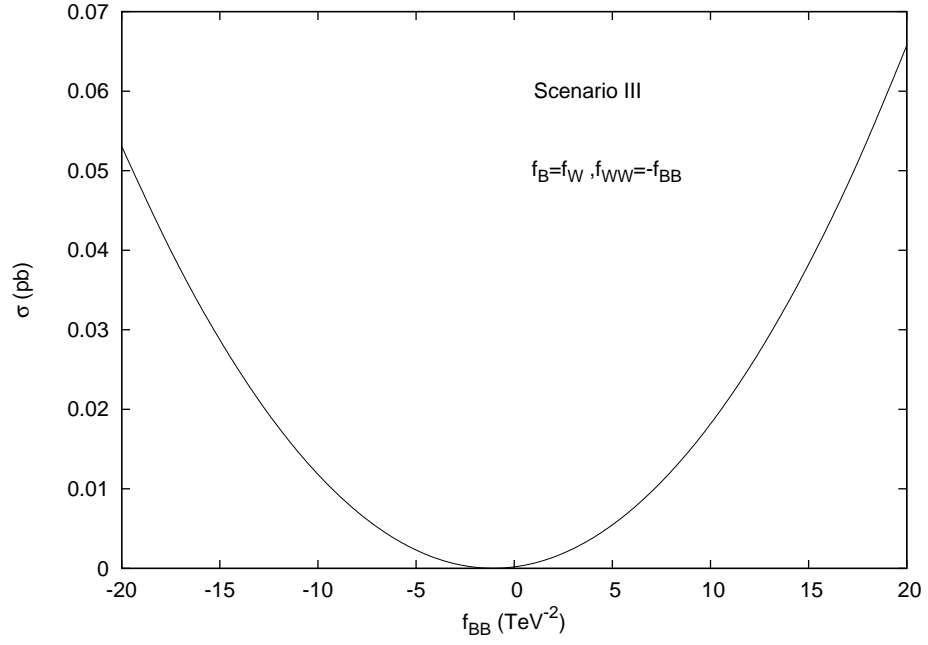


FIG. 5: The same as Fig.3 but for scenario III.

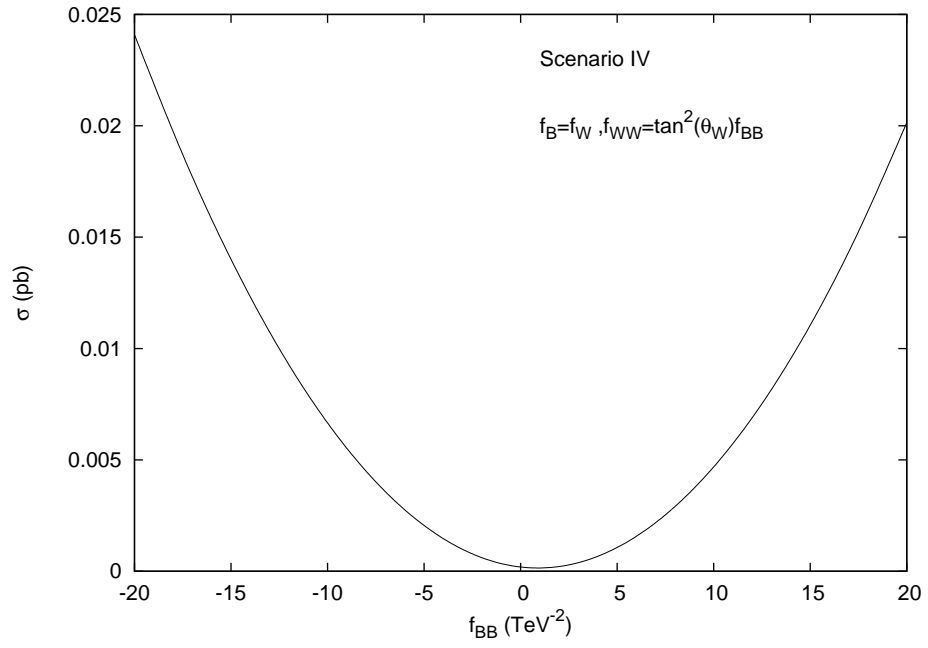


FIG. 6: The same as Fig.3 but for scenario IV.

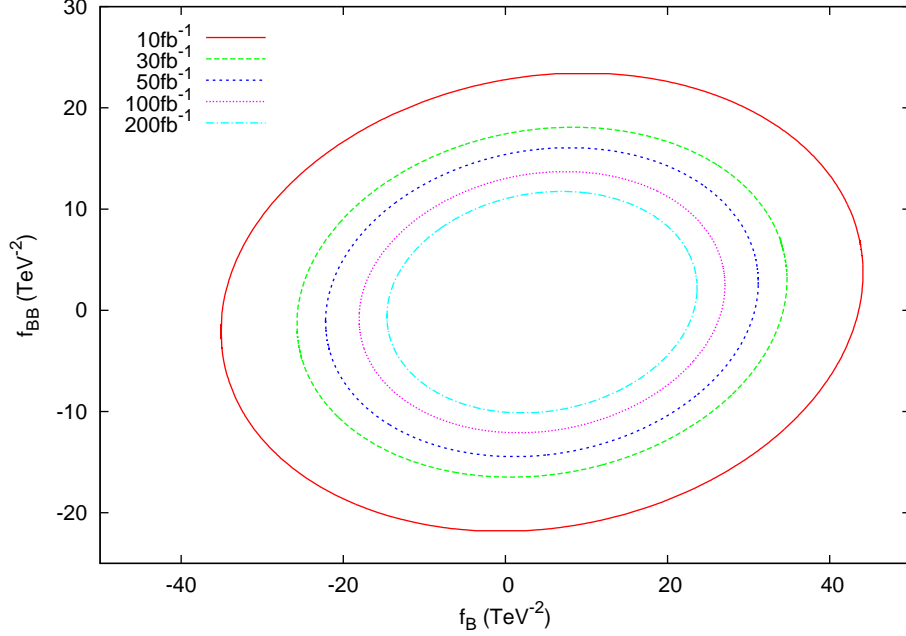


FIG. 7: The areas restricted by the lines show 95% C.L. sensitivity bounds on the parameter space $f_B - f_{BB}$ for various integrated LHC luminosities stated on the figure. The scenario V is taken into consideration. The center of mass energy of the proton-proton system is taken to be $\sqrt{s} = 14\text{TeV}$.

TABLE II: 95% C.L. bounds on f_{ww}, f_w and f_{bb} for various integrated linear collider luminosities and scenarios. Bounds are given in units of TeV^{-2} . The main e^-e^+ collider energy is taken to be $\sqrt{s} = 0.5\text{TeV}$.

Luminosity	(Scenario-I) f_{ww}	(Scenario-II) f_w	(Scenario-III) f_{bb}	(Scenario-IV) f_{bb}
$10fb^{-1}$	(-0.8,1.3)	(-7.6,3.4)	(-3.8,1.7)	(-1.3,2.0)
$30fb^{-1}$	(-0.5,1.1)	(-6.5,2.3)	(-3.2,1.2)	(-1.0,1.6)
$50fb^{-1}$	(-0.5,1.0)	(-6.1,1.9)	(-3.0,1.0)	(-0.8,1.5)
$100fb^{-1}$	(-0.4,0.9)	(-5.6,1.5)	(-2.8,0.7)	(-0.6,1.3)
$200fb^{-1}$	(-0.3,0.9)	(-5.3,1.1)	(-2.6,0.6)	(-0.5,1.2)

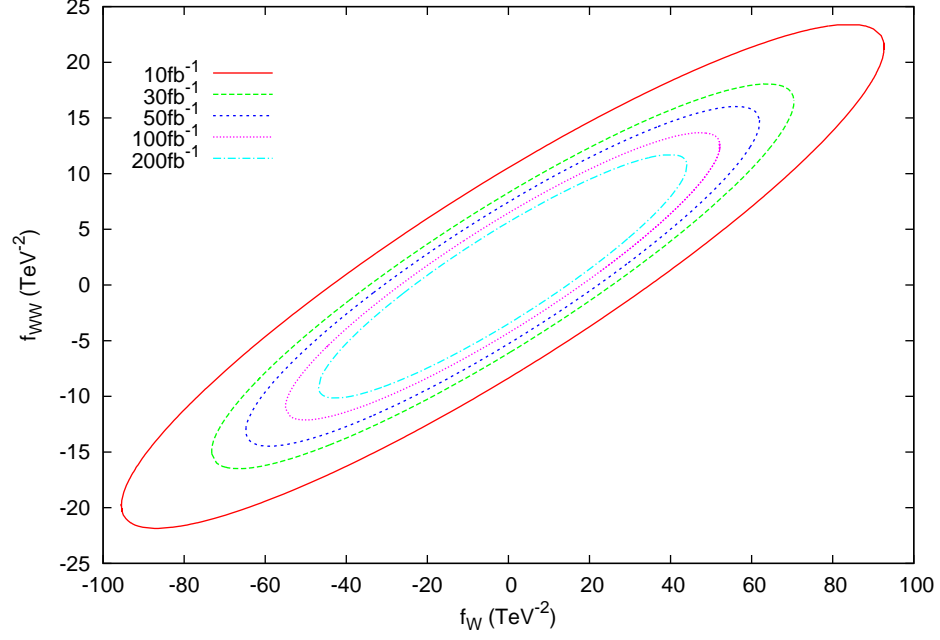


FIG. 8: The areas restricted by the lines show 95% C.L. sensitivity bounds on the parameter space $f_W - f_{WW}$ for various integrated LHC luminosities stated on the figure. The scenario VI is taken into consideration. The center of mass energy of the proton-proton system is taken to be $\sqrt{s} = 14\text{TeV}$.

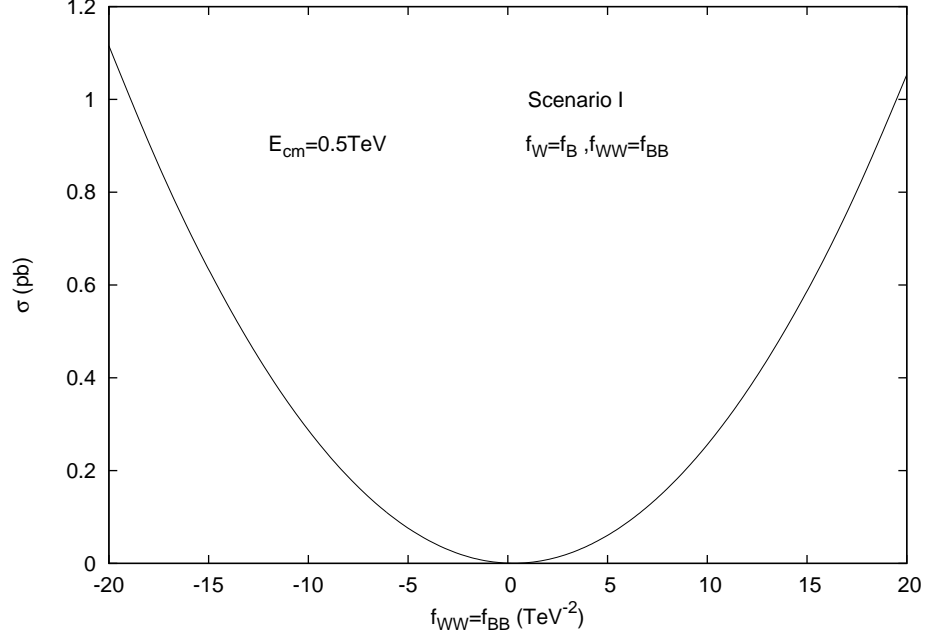


FIG. 9: The total cross section observed in the e^-e^+ collision as a function of non-standard Higgs coupling for scenario I. The main e^-e^+ collider energy is taken to be $\sqrt{s} = 0.5\text{TeV}$.

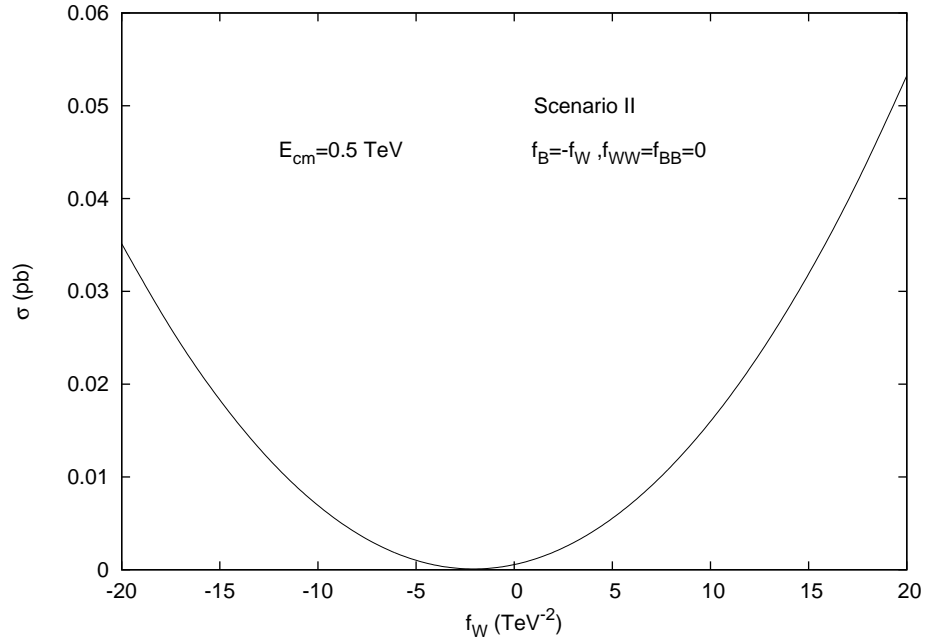


FIG. 10: The same as Fig.9 but for scenario II.

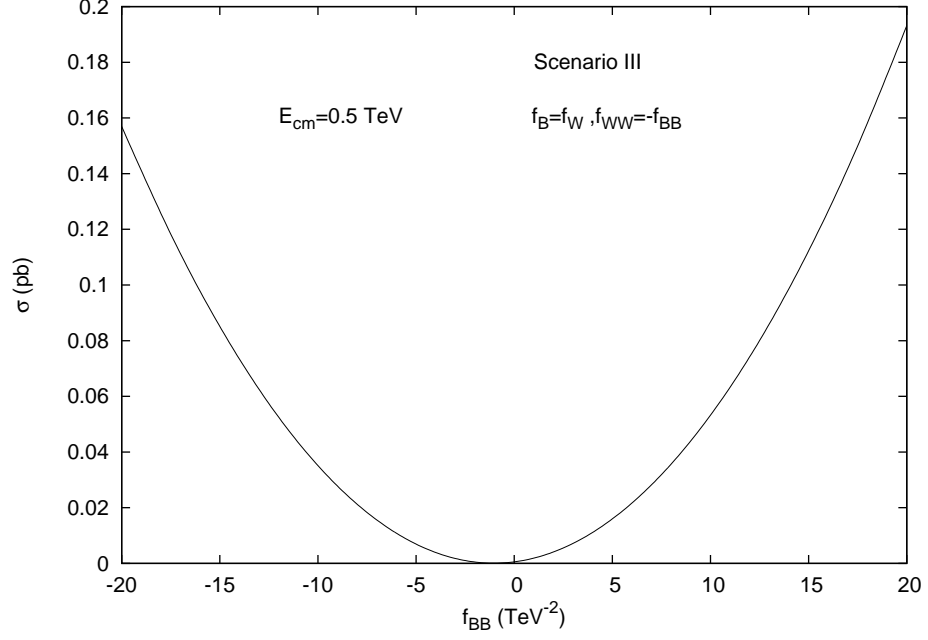


FIG. 11: The same as Fig.9 but for scenario III.

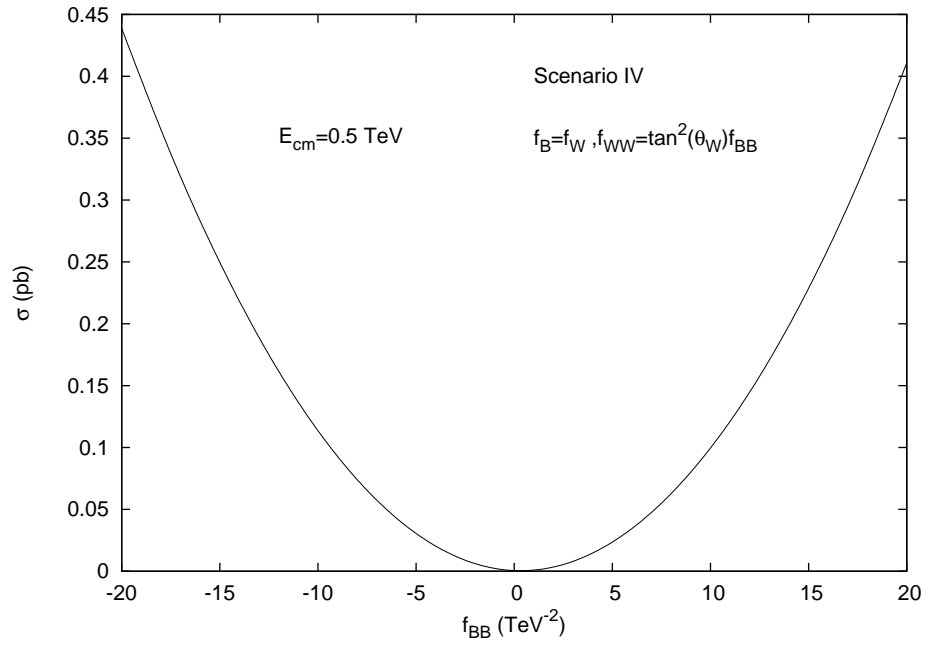


FIG. 12: The same as Fig.9 but for scenario IV.

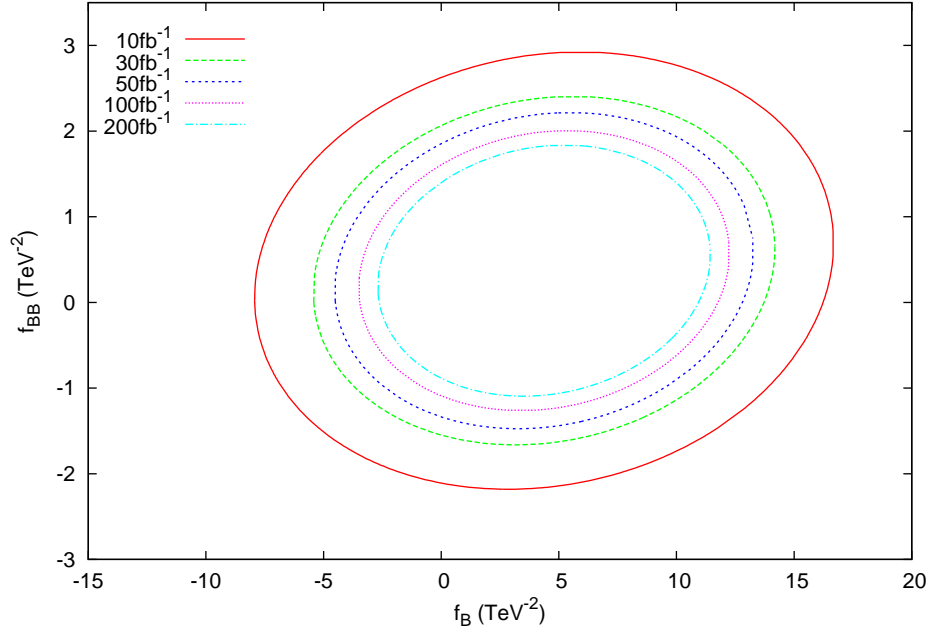


FIG. 13: The areas restricted by the lines show 95% C.L. sensitivity bounds on the parameter space $f_B - f_{BB}$ for various integrated linear collider luminosities stated on the figure. The scenario V is taken into consideration. The main e^-e^+ collider energy is taken to be $\sqrt{s} = 0.5\text{TeV}$.

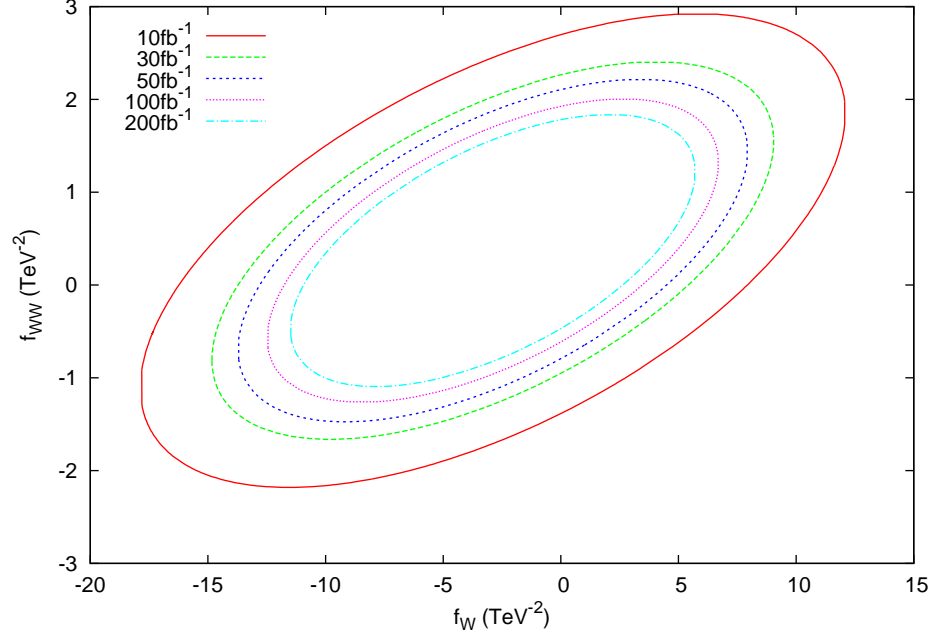


FIG. 14: The areas restricted by the lines show 95% C.L. sensitivity bounds on the parameter space $f_W - f_{WW}$ for various integrated linear collider luminosities stated on the figure. The scenario VI is taken into consideration. The main e^-e^+ collider energy is taken to be $\sqrt{s} = 0.5\text{TeV}$.